Chapter 4

Adaptive Asymptotic Performance with Indefinite Control Coefficient and Adjustable Parameters in Power System

In power system networks, time-varying parameters of the synchronous generator may lead to instability under disturbances. Therefore, an adequate control strategy is required against parametric uncertainties, especially those associated with the control input. This chapter of the thesis uses the Nussbaum function for time-varying indefinite control coefficient (ICC) in synchronous generators (SGs). In the proposed control scheme, an error-reliant tracking normalized function & barrier function is used for global performance with adaptive asymptotic tracking of synchronous generator states. The state error boundaries and adaptive laws for unknown parameters with super twisting law in backstepping control are designed. Recursive error due to virtual control design in the backstepping method is compensated through a filter design. The stability of the power system network is ensured with the control law formulation of the Lyapunov function. Compared with the existing control schemes, the proposed control guarantees transient accuracy and fast-tracking performance. The proposed controller's efficacy is performed by simulation in MATLAB and real-time digital simulator (RTDS) on IEEE standard New England 39-bus, 10-machine power system model.

4.1 Introduction

Power system operation in a multimachine is inherently stable, but the transient operation may be affected due to disturbances and parametric uncertainties. Unknown power system parameters may also affect the power system stability during transient perturbations. These parameters must be tuned adaptively to compensate for uncertainties in the power system operation. The controller performance may deviate if these unknown parameters are the control input coefficients. The performance of excitation controllers mainly

depends on the synchronous generator's dynamical models.

Conventionally, power systems stabilizers (PSSs) provide extra damping to improve stability and damp out low-frequency oscillations. But these usually perform well against small perturbations like minor load demand variations [44]. Under large perturbations, the PSSs may not offer effective damping to suppress low-frequency oscillations [44]. Various innovative linear control schemes, like linear quadratic regulator (LQR) and H_∞ based controllers, were proposed in [46], and [60] to overcome the PSSs limitations, but these linear schemes are restricted to retain the power system stability to fixed operating points.

Other renowned linear methods for power system networks are proposed in [61] and [62]. In these schemes, adaptation for power system nonlinearities is obtained through recurrent neural networks and generalized neural networks with the integration of PSSs, respectively. These schemes show a strong potential for implementation toward the physical system, although has some limitations due to the neural network's long-term learning dependency.

Nonlinear controllers are therefore presented in [25],[63]-[66] based on feedback linearization, sliding mode control (SMC), and backstepping techniques. The feedback linearized control includes direct, exact, and partial feedback linearization control. In direct and exact methods, an extra observer is required to measure the rotor angle in the control design [11]. On the other hand, in a partial feedback linearization scheme, the rotor angle is not taken as a feedback signal and hence avoids the observer implementation. But this control scheme cannot cover the aspects of unknown parameters in the power system dynamics [19]. Robust schemes like SMC were introduced to overcome these parametric sensitivity issues in the feedback linearization schemes. The SMC technique is robust in mitigating the impact of external disturbances [17], [25] ,[66]. However, the presence of chattering remains a significant issue. Also, an adequate sliding surface for power system dynamics is a challenging issue. Similarly, the optimal scheme presented in [18] has problems with the perfect design of optimal cost function for the interconnected nonlinear power system dynamics. An adaptive backstepping method is a

robust control strategy to retain transient stability under external disturbances, enabling unknown parameter estimation using adaptation laws [67], [68].

In [69], [70], an adaptive backstepping method is implemented to build excitation controllers in which the damping coefficient was assumed to be unknown. Another similar technique [71] treated the synchronous generator's transient reactance and damping coefficient as unknowns, whereas other power system unknown parameters have not been considered in [69]– [71]. The adaptive backstepping scheme in [72] has considered parametric uncertainties while designing the control law. In the robust adaptive backstepping schemes [36] and [42], unknown parameters' sensitivity to the system stability was discussed in detail. Additionally, it clarifies the importance of the impact of unknown parameters in a multimachine power system with a more meaningful vision. It was shown in [36] and [42] that the variations in power system parameters in a specified range significantly affect the multimachine state trajectories. Therefore, to counter this impact, the dynamic tuning of these parameters is essential with an adaptation law. In both [36] and [42], the adaptation law was designed using many internal signals, enhancing the complexity and sensitivity of the adaptation law towards the changes in internal signals.

In the considerable work [74]-[76], exploring the backstepping design of excitation control is accomplished. The ref. [73], discusses the control complexity suppression inherent in the conventional back-stepping design. Whereas [74] exploits the use of optimal control with suitable cost functions for obtaining adaptive laws of the system parameters. In [75], the fuzzy wavelet neural network technique is designed for the adaptive law associated with the auxiliary equations in the context of wave rider vehicles. Apart from these schemes, the proposed control incorporates normalized and barrier functions for the global stability of the closed-loop interconnected power system network, which is integrated with super twisting law to enhance the disturbance rejection capability. In the proposed scheme, simplified and systematic adaptive tuning laws are designed for the unknown system parameters along with the unknown control coefficient. In backstepping algorithms, the recursive additive error in the virtual control law may

cause deviation from the desired equilibrium in the control performance. In the proposed scheme, an attempt is made to address these concerns, including the indefinite control coefficient sequentially. In the control design for a complex interconnected network, the control function formulation becomes more complex whenever the control signal is attached with an unknown magnitude coefficient. This is because the uncertain magnitude of the control coefficient may worsen the system performance and lead the system toward an undesired trajectory. Changing the control force magnitude in an adaptive form is preferable to pursue this control objective due to variation in the unknown control coefficient. At an improper gain, the controller may deteriorate the system's behavior. However, it is possible to immediately adjust the control parameter to achieve the required state through the Nussbaum function [76], [77].

Various applications of the Nussbaum function association with unknown control coefficients are presented in [78]-[82]. In ref. [78] the Nussbaum function is utilized in a multiagent formulation to resolve the issues associated with unknown control direction. In ref. [79], the Nussbaum function is applied with adaptive neural network control, whereas in [80], multiple unknown control directions are explored. In the ref. [81], the Nussbaum function is studied for the nonlinear system's prescribed global performance, and in [82] Nussbaum function is used for reduced computation strategy for improved tracking performance.

In the power system, the indefinite control coefficient associated with the excitation control needs to be investigated using the Nussbaum function approach. Therefore, a Nussbaum function is used in control law formulation with a positive Lyapunov candidate to ensure the boundedness of the Lyapunov candidate and hence the system stability. The proposed control scheme contributes with the following merits to the advancement of an adaptive backstepping method for a multimachine power system network:

- The proposed control technique provides global adaptive asymptotic tracking that can guarantee boundedness during the transient performance under uncertainties. A tracking error-reliant normalized and a barrier function is developed that incorporates time-dependent scaling transformation. As a result, enhanced

performance with the following features is achieved:

I. Adaptive tuning assures asymptotic accuracy.

II. Adaptation against unknown control coefficients, power system nonlinearities, and mismatched uncertainties are ensured.

- Simplified adaptive tuning laws are designed to estimate unknown parameters.
- The super twisting law is implemented with a backstepping scheme to provide strong disturbance rejection and robustness to the system under perturbations.
- A filter is designed via state errors to compensate for a recursive error produced due to virtual control formulation in the backstepping scheme.

4.2 Power System Dynamics for Control Strategy and Problem Formulation

In a multimachine system, synchronous generators (SGs) are interconnected to satisfy the load demand. The excitation control of SGs in a multimachine power system can be modeled based on 3rd-order dynamics (*2.1*)-(*2.3*) as provided in chapter 2. The dynamics are configured by including both mechanical and electrical dynamics of i^{th} SGs in the network have n generators. Dynamics of SGs in the electromechanical sense are represented with their parameters having usual meanings in the differential equations (*2.1*) & (*2.2*) [69], [36] explained in chapter 2. Eqns. (*2.1*) & (*2.2*) in the chapter 2 represent the SG's mechanical dynamics while eqn. (*2.3*) represents the electrical dynamics of the SG. For the generator control, input is the field voltage and outputs are speed deviation and terminal voltage (V_t). The overall plant dynamics is treated as electrical and mechanical parts separately. For the electrical part, input constitutes excitation field voltage. The measurable electrical output is stator current, damper winding current, field current and stator voltage. Similarly, for the mechanical part, input constitutes the mechanical power (through governor) and output is the incremental speed deviation from nominal value and incremental rotor angle deviation.

The electrical equations with their usual meaning can be presented in eqns. (*2.4*)-(*2.9*) of chapter 2 [69],[36]. With this, eqns. (*2.1*)-(*2.3*) can be rearranged as in eqns. (*2.10*)-(*2.12*) which is provided in chapter 2. Now from these eqns. (*2.10*)-(*2.12*) an adaptive

backstepping excitation control law E_{fdi} can be designed by modifying eqns. (*2.10*)-(*2.12*) and rewriting as:

$$\dot{x}_1 = x_2 \tag{4.1}$$

$$\dot{x}_2 = \theta_1 x_2 + \theta_2 P_{mi} - \theta_2 I_{qi} x_3 \tag{4.2}$$

$$\dot{x}_3 = -\theta_3 x_3 - \theta_4 I_{di} + \theta_3 U \tag{4.3}$$

$$y = \Delta x_2 \tag{4.4}$$

The variables x_1, x_2 and x_3 are state variables δ, ω and E'_{qi}, respectively. Also, $\theta_1 = -\frac{D_i}{2H_i}$, $\theta_2 = \frac{\omega_{0i}}{2H_i}$, $\theta_3 = \frac{1}{T_{doi}}$, $\theta_4 = \frac{(x_{di} - x'_{di})}{T_{doi}}$ and control input $U = E_{fdi}$. Here the first state error e_1 is defined as $x_1 - y_d$. Where $'y_d'$ represents the desired reference value of initial rotor angle state and the output function for each generator is represented as 'y'.

Now the normalized function $\mathrm{F}(\boldsymbol{e_1})$ with error $\boldsymbol{e_1}$ is defined as [74]:

$$\mathrm{F}(e_1) = \frac{e_1}{\sqrt{{e_1}^2 + l}} \tag{4.5}$$

where l is a positive constant. It can be observed from (*4.5*) that $\mathrm{F}(e_1)$ exhibits the following characteristics:

- $\mathrm{F}(e_1) \in (-1, 1)$ for $\forall\ e_1 \in R$.
- $\mathrm{F}(e_1) \to 1$ for $e_1 \to \infty$.
- $\mathrm{F}(e_1) \to -1$ for $e_1 \to -\infty$.
- $\mathrm{F}(e_1) = 0$ for $e_1 = 0$.
- $\mathrm{F}(e_1)$ is firmly monotonical concerning $e_1 \in R$.

Now, to tune error tracking, a function $\zeta(t)$ is defined for a time-varying scaling function $\beta(t)$:

$$\zeta(t) = \beta(t)\mathrm{F}(e_1) \tag{4.6}$$

For global adaptive asymptotic tracking of state x_1, the error z_1 can be written in the form of the barrier function 's' as:

$$z_1 = s = \frac{\zeta(t)}{1 - \zeta(t)^2} \tag{4.7}$$

Further other state errors can be expressed as follows:

$$z_2 = x_2 - \propto_1 \quad 4.8$$

$$z_3 = x_3 - \propto_2 \quad 4.9$$

Where $\propto_1$ and $\propto_2$ are the designed vertual control inputs in the proposed backstepping control scheme. The proposed controller is designed through the following steps:

Step 1: By calculating the first step error derivative $\dot{z}_1$ as:

$$\dot{z}_1 = \dot{s} = \frac{1-\zeta^2}{(1-\zeta^2)^2}\dot{\zeta} = \mu\dot{\zeta} \quad 4.10$$

$$\dot{\zeta} = \dot{\beta}\mathrm{F} + \dot{\mathrm{F}}\beta \quad 4.11$$

$$\dot{\mathrm{F}} = \frac{l}{\sqrt{{e_1}^2 + l}({e_1}^2 + l)}\dot{e_1} = \rho\dot{e_1} \quad 4.12$$

where $\mu = \frac{1+\zeta^2}{(1-\zeta^2)^2}$ and $\rho = \frac{l}{\sqrt{{e_1}^2+l}({e_1}^2+l)}$.

Now,

$$\dot{z}_1 = \mu\dot{\beta}\mathrm{F} + \mu\beta\rho\dot{e_1} \quad 4.13$$

$$\dot{z}_1 = \mu\dot{\beta}\mathrm{F} + \mu\beta\rho(\dot{x}_1 - \dot{y}_d) \quad 4.14$$

$$\dot{z}_1 = \mu\dot{\beta}\mathrm{F} + \mu\beta\rho(z_2 + \propto_1 - \dot{y}_d) \quad 4.15$$

$$\dot{z}_1 = \mu_1(z_2 + \propto_1) - \mu_1\dot{y}_d + \mu_2 \quad 4.16$$

where $\mu_1 = \mu\beta\rho$ and $\mu_2 = \mu\dot{\beta}\mathrm{F}$.

Nussbaum function: A Nussbaum function is applied in formulating an adaptive control law design to deal with the indefinite control coefficient. An unknown control coefficient signifies a time-dependent control coefficient of unknown magnitude. The Nussbaum function is defined as:

Definition 1: A function $\mathrm{h(s)}: [0, \infty) \rightarrow (-\infty, \infty)$ which is continuously differentiable is known as the Nussbaum function if:

$$\lim_{y\to\infty}\sup\frac{1}{y}\int_0^y h(s)ds = \infty \quad 4.17$$

$$\lim_{y\to\infty}\inf\frac{1}{y}\int_0^y h(s)ds = -\infty \quad 4.18$$

The Nussbaum function offers control gain with a rising magnitude. The Nussbaum function is considered in the following form.

$$h(s) = \sin(s)\ e^{s^2} \tag{4.19}$$

Lemma 1: Let a positive Lyapunov function $V(t) \geq 0$ and $\wp(t)$ be defined on $[0, t_f)$ for $\forall t \in [0, t_f)$; The $h(\cdot)$ is defined as Nussbaum like function, and q_0 as a real constant. Now if $V(t) \leq \left\{\int_0^{t_0}\left[q_0 h\left(\wp(\tau)\right) + 1\right]\dot{\wp}(\tau)d\tau + \text{const}\right\}$ holds, then $V(t), \wp(t)$ and $\int_0^{t_0}\left[q_0 h\left(\wp(\tau)\right) + 1\right]\dot{\wp}(\tau)d\tau$ must be bounded on $[0, t_f)$.

Now defining $\propto_1$ as:

$$\propto_1 = h(\chi_1)\ \bar{\propto}_1 \tag{4.20}$$

Eqn. (*4.16*) can therefore be rewritten as:

$$\dot{z}_1 = \mu_1 z_2 + \mu_1 h(\chi_1)\ \bar{\propto}_1 - \mu_1 \dot{y}_d + \mu_2 \tag{4.21}$$

Further defining $\bar{\propto}_1$ as:

$$\bar{\propto}_1 = \frac{1}{\mu_1}\left(k_{1a}|z_1|^{1/2} sgn(z_1) - \mu_{1a} - \mu_1 \dot{y}_d + \mu_2\right) \tag{4.22}$$

Placing value of $\bar{\propto}_1$ from (*4.22*) in (*4.21*), the $\dot{z}_1$ is obtained as:

$$\dot{z}_1 = \mu_1 z_2 + \mu_1 (h(\chi_1) + 1)\ \bar{\propto}_1 - k_{1a}|z_1|^{1/2} sgn(z_1) + \mu_{1a} \tag{4.23}$$

Stability analysis for step 1: For the stability study of error z_1, a positive Lyapunov candidate v_1 is defined as:

$$v_1 = \frac{1}{2}{\mu_{1a}}^2 + k_{1b}|z_1| \tag{4.24}$$

Taking derivative of v_1 with $\dot{\mu}_{1a} = -k_{1b} sgn(z_1)$ is as:

$$\begin{aligned} \dot{v}_1 = {} & -k_{1b}\mu_{1a} sgn(z_1) - k_{1a}k_{1b}|z_1|^{1/2} + k_{1b}\mu_{1a} sgn(z_1) \\ & + \mu_1 z_2 k_{1b} sgn(z_1) \\ & + k_{1b}\mu_1 (h(\chi_1) + 1)\ \bar{\propto}_1\ sgn(z_1) \end{aligned} \tag{4.25}$$

Now introducing a tuning function χ_1 which is estimated as:

$$\dot{\chi}_1 = \gamma_1 k_{1b}\mu_1\ \bar{\propto}_1\ sgn(z_1) \tag{4.26}$$

From eqns. (*4.25*)-(*4.26*) $\dot{v}_1$ can be written as:

$$\dot{v}_1 = -k_{1a}k_{1b}|z_1|^{1/2} + \mu_1 z_2 k_{1b} sgn(z_1) + \frac{1}{\gamma_1}(h(\chi_1) + 1)\dot{\chi}_1 \tag{4.27}$$

$$\dot{v}_1 + k_{1a}k_{1b}|z_1|^{1/2} = \mu_1 z_2 k_{1b} sgn(z_1) + \frac{1}{\gamma_1}(h(\chi_1) + 1)\dot{\chi}_1 \quad 4.28$$

Taking integral at both sides of eqn. (*4.28*).

$$v_1 + c_1 \int_0^t k_{1a}k_{1b}|z_1|^{1/2} = \frac{1}{\gamma_1}\int_0^t (h(\chi_1) + 1)\dot{\chi}_1 + \Xi_1 \quad 4.29$$

where $\Xi_1 = v_1(0) + \lambda_1$ and $\int_0^t \mu_1 z_2 k_{1b} sgn(z_1) \leq \lambda_1$. Eqn. (*4.29*) will therefore satisfy lemma 1.

Step 2: The second virtual control $\propto_2$ can be designed by calculating the derivative of second state error z_2 as:

$$\dot{z}_2 = \theta_1 x_2 + \theta_2 P_m - \theta_2 I_q z_3 - \theta_2 I_q \propto_2 - \frac{\partial \propto_1}{\partial x_1} x_2 - \sum_{k=0}^{1} \frac{\partial \propto_1}{\partial y_d^k} y_d^{k+1} - \sum_{k=0}^{1} \frac{\partial \propto_1}{\partial \beta^k} \beta^{k+1} - \sum_{k=0}^{1} \frac{\partial \propto_1}{\partial \chi_1} \dot{\chi}_1 \quad 4.30$$

Defining $\propto_2 = h(\chi_2)\ \overline{\propto}_2$ and $\overline{\propto}_2$ as:

$$\overline{\propto}_2 = \frac{1}{\theta_2 I_q}\left[\hat{\theta}_1 x_2 + \hat{\theta}_2 P_m + k_{2a}|z_2|^{1/2} sgn(z_2) - \mu_{2a} - \frac{\partial \propto_1}{\partial x_1} x_2 - \sum_{k=0}^{1} \frac{\partial \propto_1}{\partial y_d^k} y_d^{k+1} - \sum_{k=0}^{1} \frac{\partial \propto_1}{\partial \beta^k} \beta^{k+1} - \sum_{k=0}^{1} \frac{\partial \propto_1}{\partial {\chi_1}^k} \dot{\chi}_1\right] \quad 4.31$$

From (*4.30*) and (*4.31*), $\dot{z}_2$ can be written as:

$$\dot{z}_2 = -k_{2a}|z_2|^{1/2} sgn(z_2) + \mu_{2a} + \tilde{\theta}_1 x_2 + \tilde{\theta}_2 P_m - \theta_2 I_q z_3 - \theta_2 I_q (h(\chi_2) - 1)\ \overline{\propto}_2 \quad 4.32$$

Stability analysis for step 2: For the stability study of error z_2 another positive Lyapunov candidate v_2 is defined as:

$$v_2 = \frac{1}{2}{\mu_{2a}}^2 + k_{2b}|z_2| + \frac{1}{2}\tilde{\theta}_1 {\Gamma_1}^{-1}\tilde{\theta}_1 + \frac{1}{2}\tilde{\theta}_2 {\Gamma_2}^{-1}\tilde{\theta}_2 \quad 4.33$$

Taking derivative of v_2 with $\dot{\mu}_{2a} = -k_{2b} sgn(z_2)$ is as:

$$\dot{v}_2 = -\mu_{2a}k_{2b} sgn(z_2) + k_{2b} sgn(z_2)\left[-k_{2a}|z_2|^{1/2} sgn(z_2) + \mu_{2a} + \tilde{\theta}_1 x_2 + \tilde{\theta}_2 P_m - \theta_2 I_q z_3 - \theta_2 I_q (h(\chi_2) - 1)\ \overline{\propto}_2\right] + \tilde{\theta}_1 {\Gamma_1}^{-1}\dot{\hat{\theta}}_1 + \tilde{\theta}_2 {\Gamma_2}^{-1}\dot{\hat{\theta}}_2$$

$$\begin{aligned}\dot{v}_2 = -k_{2a}k_{2b}|z_2|^{1/2} - \theta_2 I_q z_3 k_{2b} sgn(z_2) + \tilde{\theta}_1 x_2 k_{2b} sgn(z_2) \\ + \tilde{\theta}_2 P_m k_{2b} sgn(z_2) \\ - \theta_2 I_q k_{2b}(h(\chi_2) - 1)\ \overline{\propto}_2\ sgn(z_2) - \tilde{\theta}_1 \Gamma_1^{-1}\dot{\hat{\theta}}_1 \\ - \tilde{\theta}_2 \Gamma_2^{-1}\dot{\hat{\theta}}_2\end{aligned} \quad 4.34$$

Further, a tuning function χ_2 is estimated as:

$$\dot{\chi}_2 = \gamma_2 \theta_2 I_q k_{2b}\ \overline{\propto}_2\ sgn(z_2) \quad 4.35$$

and adaptive tuning law for parameters $\hat{\theta}_1$ and $\hat{\theta}_2$ as:

$$\begin{aligned}\dot{\hat{\theta}}_1 = \Gamma_1 x_2 k_{2b} sgn(z_2) \\ \dot{\hat{\theta}}_2 = \Gamma_2 P_m k_{2b} sgn(z_2)\end{aligned} \quad 4.36$$

From eqns. (*4.34*), (*4.35*), and (*4.36*), $\dot{v}_2$ can be simplified as:

$$\begin{aligned}\dot{v}_2 = -k_{2a}k_{2b}|z_2|^{1/2} - \frac{1}{\gamma_2}\big((h(\chi_2) - 1)\big)\dot{\chi}_2 \\ - \theta_2 I_q z_3 k_{2b} sgn(z_2)\end{aligned} \quad 4.37$$

By taking both sides integral in (*4.37*),

$v_2 + c_2 \int_0^t k_{2a}k_{2b}|z_2|^{1/2} = \frac{1}{\gamma_2}\int_0^t \big(1 - h(\chi_2)\big)\dot{\chi}_2 + \Xi_2$

where $\Xi_2 = v_2(0) - \lambda_2$ and $\int_0^t \theta_2 I_q z_3 k_{2b} sgn(z_2) \leq \lambda_2$. The eqn. (*4.37*) will therefore satisfy lemma 1.

Step 3: The control input U is designed by calculating the derivative of the third state error z_3 as:

$$\begin{aligned}\dot{z}_3 = -\theta_3 x_3 + \theta_4 I_{di} + \theta_3 U - \sum_{k=0}^{2} \frac{\partial\ \propto_2}{\partial x_n^k} x_n^{k+1} - \sum_{k=0}^{2} \frac{\partial\ \propto_2}{\partial y_d^k} y_d^{k+1} \\ - \sum_{k=0}^{2} \frac{\partial\ \propto_2}{\partial \beta^k} \beta^{k+1} - \sum_{k=0}^{2} \frac{\partial\ \propto_2}{\partial \chi_n^k} \chi_n^{k+1} - \frac{\partial\ \propto_2}{\partial \hat{\theta}_1}\dot{\hat{\theta}}_1 \\ - \frac{\partial\ \propto_2}{\partial \hat{\theta}_2}\dot{\hat{\theta}}_2\end{aligned} \quad 4.38$$

where $n = 1,2$.

Defining U as:

$$U = h(\chi_3)\overline{U} \tag{4.39}$$

and $\overline{U}$ as:

$$\begin{aligned}\overline{U} = \frac{1}{\theta_3}\Bigg[&-k_{3a}|z_3|^{1/2}sgn(z_3) + \mu_{3a} - \hat{\theta}_3 x_3 + \hat{\theta}_4 I_d \\ &- \sum_{k=0}^{2}\frac{\partial \propto_2}{\partial x_n^k}x_n^{k+1} - \sum_{k=0}^{2}\frac{\partial \propto_2}{\partial y_d^k}y_d^{k+1} \\ &- \sum_{k=0}^{2}\frac{\partial \propto_2}{\partial \beta^k}\beta^{k+1} - \sum_{k=0}^{2}\frac{\partial \propto_2}{\partial \chi_n^k}\chi_n^{k+1} - \frac{\partial \propto_2}{\partial \hat{\theta}_1}\dot{\hat{\theta}}_1 \\ &- \frac{\partial \propto_2}{\partial \hat{\theta}_2}\dot{\hat{\theta}}_2\Bigg]\end{aligned} \tag{4.40}$$

From eqns. (*4.38*) and (*4.40*) $\dot{z}_3$ can be written as:

$$\begin{aligned}\dot{z}_3 = &-k_{3a}|z_3|^{1/2}sgn(z_3) + \mu_{3a} - \tilde{\theta}_3 x_3 + \tilde{\theta}_4 I_d \\ &+ \theta_3(h(\chi_3) + 1)\overline{U}\end{aligned} \tag{4.41}$$

Stability analysis for step 3: For the stability study of error z_3, the third positive Lyapunov candidate v_3 is defined as:

$$v_3 = \frac{1}{2}{\mu_{3a}}^2 + k_{3b}|z_3| + \frac{1}{2}\tilde{\theta}_3{\Gamma_3}^{-1}\tilde{\theta}_3 + \frac{1}{2}\tilde{\theta}_4{\Gamma_4}^{-1}\tilde{\theta}_4 \tag{4.42}$$

Taking derivative of v_3 with $\dot{\mu}_{3a} = -k_{3b}sgn(z_3)$ is as:

$$\begin{aligned}\dot{v}_3 = &-\mu_{3a}k_{3b}sgn(z_3) \\ &+ k_{3b}sgn(z_3)\left[-k_{3a}|z_3|^{1/2}sgn(z_3) + \mu_{3a} - \tilde{\theta}_3 x_3 + \tilde{\theta}_4 I_d\right. \\ &\left.+ \theta_3(h(\chi_3) + 1)\overline{U}\right] - \tilde{\theta}_3{\Gamma_3}^{-1}\dot{\hat{\theta}}_3 + \tilde{\theta}_4{\Gamma_4}^{-1}\dot{\hat{\theta}}_4\end{aligned}$$

$$\begin{aligned}\dot{v}_3 = &-k_{3a}k_{3b}|z_3|^{1/2} - \tilde{\theta}_3 x_3 k_{3b}sgn(z_3) + \tilde{\theta}_4 I_d k_{3b}sgn(z_3) \\ &+ \theta_3 k_{3b}(h(\chi_3) + 1)\overline{U}sgn(z_3) - \tilde{\theta}_3{\Gamma_3}^{-1}\dot{\hat{\theta}}_3 \\ &+ \tilde{\theta}_4{\Gamma_4}^{-1}\dot{\hat{\theta}}_4\end{aligned} \tag{4.43}$$

Further, introducing the tuning function χ_3, that is estimated as:

$$\dot{\chi}_3 = \gamma_3\theta_3 k_{3b}\overline{U}sgn(z_3) \tag{4.44}$$

and adaptive tuning law for parameters $\hat{\theta}_3$ and $\hat{\theta}_4$ as:

$$\dot{\hat{\theta}}_3 = -\Gamma_3 x_3 k_{3b} sgn(z_3)$$
$$\dot{\hat{\theta}}_4 = \Gamma_4 I_d k_{3b} sgn(z_3) \quad 4.45$$

From eqns. (*4.43*), (*4.44*), and (*4.45*), $\dot{v}_3$ can be simplified as:

$$\dot{v}_3 = -k_{3a} k_{3b} |z_3|^{1/2} + \frac{1}{\gamma_3}\left((h(\chi_3) + 1)\right)\dot{\chi}_3 \quad 4.46$$

By taking both sides integral in (*4.37*),

$v_3 + c_3 \int_0^t k_{3a} k_{3b} |z_3|^{1/2} = \frac{1}{\gamma_3}\int_0^t (h(\chi_3) + 1)\dot{\chi}_3 + \Xi_3$
where $\Xi_3 = v_3(0)$. Eqn. (*4.46*) will therefore satisfy lemma 1.

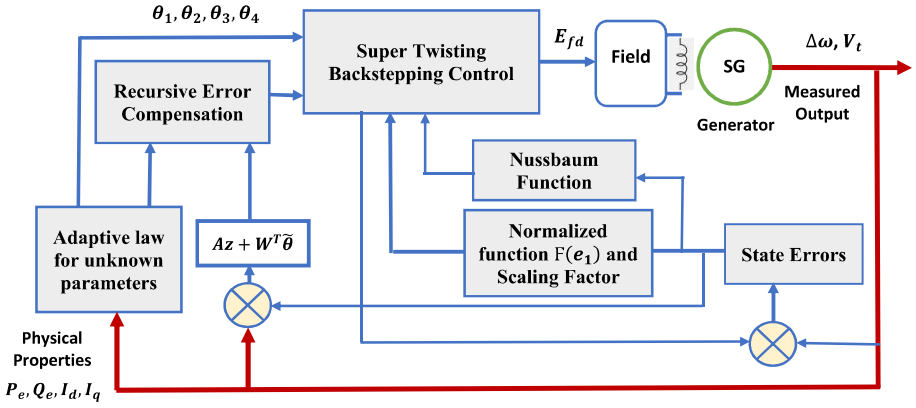

Figure 4.1. Block representation of suggested scheme.

In Figure *4.1* the implementation proposed scheme is explained. It shows that the state errors are obtained from the feedback and from the forward backstepping control outputs. These state errors are used to obtain corresponding Nussbaum and normalized function for designing the super twisting based backstepping control. Further from the control input and generator feedback signals adaptive laws for uncertain parameters are designed with the recursive error compensation algorithm.

Further the proposed control design can be extended for the higher order model of power system network. The detailed mathematics formulation of higher order dynamics is reflected with additional set of equations as mentioned in the expression (*4.47*) and (*4.48*) respectively. By taking the higher order dynamics from [31] and defining other unknown parameters θ_5, θ_6, θ_7 and θ_8 in the extension of the dynamics (*4.1*)-(*4.3*) as,

$$\dot{x}_4 = \theta_5 x_4 - \theta_6 I_{qi} \quad 4.47$$

$$\dot{x}_5 = \theta_7 x_5 + \theta_8\left(V_{refi} - V_{ti}\right) + \theta_8 U \tag{4.48}$$

where, x_4, x_5 are E'_{di} & E_{fdi}. Also, $\theta_5 = -\frac{1}{T_{qoi}}$, $\theta_6 = \frac{(x_{qi} - x'_{qi})}{T_{qoi}}$, $\theta_7 = \frac{1}{T_{Ai}}$ and $\theta_8 = \frac{K_{Ai}}{T_{Ai}}$.

The stabilization control law 'V_{ci}' can be designed as:

$$U = h(\chi_5)\overline{U} \tag{4.49}$$

where, $\overline{U} = \frac{1}{\theta_8}\Big[-k_{5a}|z_5|^{1/2}sgn(z_5) + \mu_{5a} + \hat{\theta}_7 x_5 + \hat{\theta}_8\left(V_{refi} - V_{ti}\right) - \sum_{k=0}^{2}\frac{\partial \propto_4}{\partial x_n^k}x_n^{k+1} - \sum_{k=0}^{2}\frac{\partial \propto_4}{\partial y_d^k}y_d^{k+1} - \sum_{k=0}^{2}\frac{\partial \propto_4}{\partial \beta^k}\beta^{k+1} - \sum_{k=0}^{2}\frac{\partial \propto_4}{\partial \chi_n^k}\chi_n^{k+1} - \frac{\partial \propto_4}{\partial \hat{\theta}_1}\dot{\hat{\theta}}_1 - \frac{\partial \propto_4}{\partial \hat{\theta}_2}\dot{\hat{\theta}}_2 - \frac{\partial \propto_4}{\partial \hat{\theta}_3}\dot{\hat{\theta}}_3 - \frac{\partial \propto_4}{\partial \hat{\theta}_4}\dot{\hat{\theta}}_4 - \frac{\partial \propto_4}{\partial \hat{\theta}_5}\dot{\hat{\theta}}_5 - \frac{\partial \propto_4}{\partial \hat{\theta}_6}\dot{\hat{\theta}}_6\Big]$.

The adaptive laws for θ_5, θ_6, θ_7 and θ_8 are obtained as:

$$\begin{aligned}\dot{\hat{\theta}}_5 &= -\Gamma_5 z_4 k_{4b} sgn(z_4)\\ \dot{\hat{\theta}}_6 &= -\Gamma_6 I_q k_{4b} sgn(z_4)\end{aligned} \tag{4.50}$$

$$\begin{aligned}\dot{\hat{\theta}}_7 &= -\Gamma_7 x_5 k_{5b} sgn(z_5)\\ \dot{\hat{\theta}}_8 &= -\Gamma_8\left(V_{rfi} - V_{ti}\right)k_{5b} sgn(z_5)\end{aligned} \tag{4.51}$$

And the tuning laws for intermediate functions χ_4 and χ_5, can be achieved as:

$$\dot{\chi}_4 = \gamma_4 \theta_5 k_{4b}\ \overline{\propto}_4\ sgn(z_4) \tag{4.52}$$

$$\dot{\chi}_5 = \gamma_5 \theta_8 k_{5b}\overline{U} sgn(z_5) \tag{4.53}$$

4.3 Recursive error compensation

From eqn. (*4.23*), (*4.32*), and (*4.41*), the derivative of multimachine state errors is expressed in the state space form as:

$$\dot{z} = Az + W^T\tilde{\theta} \tag{4.54}$$

$A = \begin{bmatrix} -k_{1a}|z_1|^{-1/2} & \mu_1 & 0 \\ 0 & -k_{2a}|z_2|^{-1/2} & \theta_2 I_q \\ 0 & 0 & -k_{3a}|z_3|^{-1/2} \end{bmatrix}$ and $W = [w_1, w_2, w_3]^T$.

where $w_1 = \mu_{1a} + \mu_1(h(\chi_1) + 1)\ \overline{\propto}_1$, $w_2 = \mu_{2a} + \tilde{\theta}_1 x_2 + \tilde{\theta}_2 P_m - \theta_2 I_q(h(\chi_2) - 1)\ \overline{\propto}_2$ and $w_3 = \mu_{3a} - \tilde{\theta}_3 x_3 + \tilde{\theta}_4 I_d + \theta_4(h(\chi_3) + 1)\overline{U}$.

z *−Swapping Scheme:* The filter for state error suppression as per the closed-loop system (*4.1*)-(*4.3*) can be expressed as [29],[83],[84]:

$$\dot{б}_z = A_z б_z + \Psi_z^T \hat{\theta} \quad 4.55$$

$$\dot{\Psi}_z^T = A_z \Psi_z^T + W^T \quad 4.56$$

The augmented state error is defined as:

$$\bar{z} = z + б_z \quad 4.57$$

which validates the following equation:

$$\bar{z} = \Psi_z^T \theta + \varepsilon_z \quad 4.58$$

where ε_z will decays exponentially.

Proof: The derivative of the error $\varepsilon_z = z + б_z - \Psi_z^T \theta$ in view of (*4.54*), (*4.55*), and (*4.56*), the differential equation $\dot{\varepsilon}_z = A_z \varepsilon_z$ is achieved with the initial condition $\varepsilon_z(0) = z(0) + б_z(0) - \Psi_z^T(0)\theta$. Now, by considering the A_z matrix structure, it can be concluded that ε_z will decay exponentially.

Remark 1: Because of the structure of A_z matrix, filter state Ψ_z (*4.54*), (*4.56*) is confined regardless of its input W. As Ψ_z is bounded, which permits the application of normalized and unnormalized adaptation laws as per regression (*4.58*). The overall block diagram representation of proposed excitation control scheme is shown in Figure *4.1*.

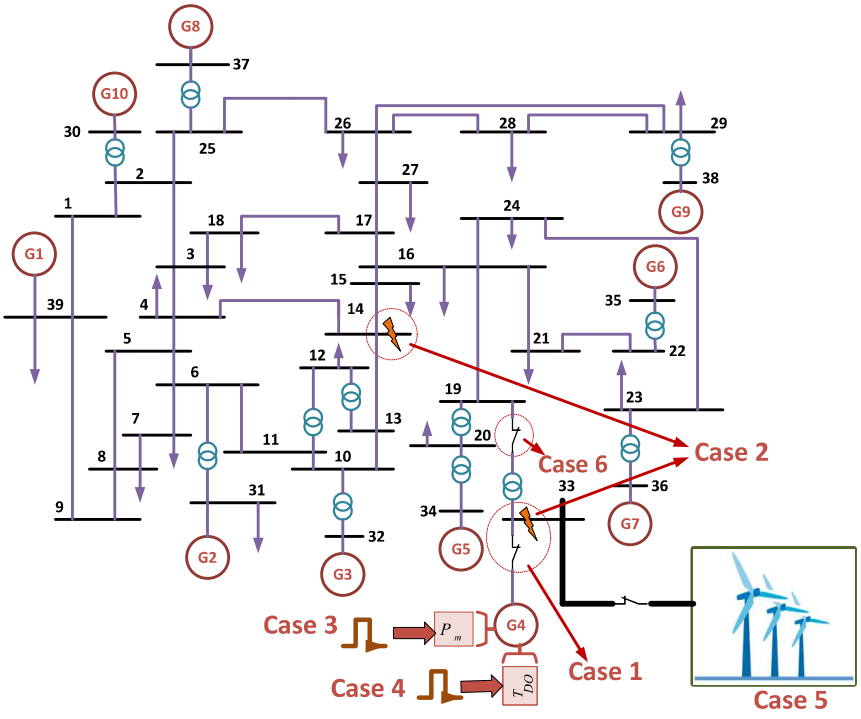

Figure 4.2. Line representation of IEEE 10 machine 39 bus power system model.

4.4 Controller verification and simulation results

The IEEE 39-bus, 10-machines New England power system model, as shown in Figure *4.2*, is used for control scheme verification. The power system model consists of both dynamic and static loads having 6150.5 MW load demand and 6193.41 MW of power generation through the ten SGs. A ± 5 pu limit is considered for all exciter's voltage to prevent the overvoltage problem. Here two-axis synchronous generator model is taken for all generators in the network. Generator-1 signifies the aggregation of the power system connected to bus 39, and a constant field voltage and mechanical torque are supplied to it. Each generator in 39 bus multimachine model is characterized as a voltage source with the source impedance of 10Ω.

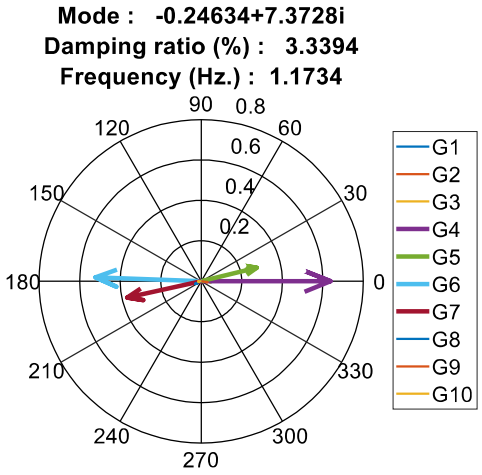

Figure 4.3. Compass plot of base system network of IEEE 39 bus system.

The corresponding transmission lines and loads are modeled using the Bergeron model and a constant PQ load. Based on the modal analysis at the base value condition, the compass plot and participation factor of the generators to least damped mode 1.17 Hz are illustrated in Figure *4.3* and Figure *4.4*, respectively. Generator $G4$ oscillates against generator $G6$, and the former generator has the highest participation factor in this mode. Thus, generator $G4$ connected to bus-33 is considered for implementation of proposed control scheme. The input-output configuration with respect to physical system is shown in Figure *4.5*.

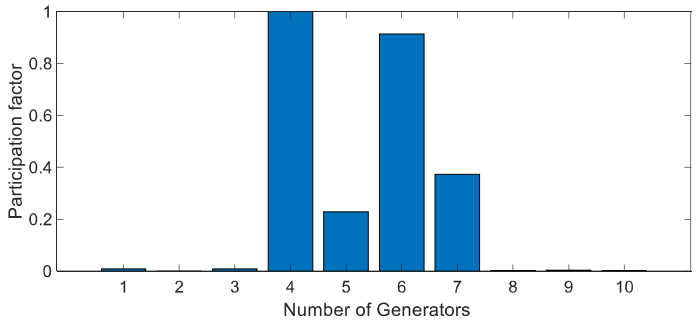

Figure 4.4. Participation factors of 10 generators in the power system network.

Specifications and Values of System Parameters

Specification	Value
$E_{min}(pu)$	$-5\ Volt$
$E_{max}(pu)$	$5\ Volt$
$V_T(pu)$	$1.03\ Volt$
H	2.86
$x'_d(pu)$	0.436
$x_d(pu)$	2.62
T'_{do}	$0.003sec$
T_{do}	$5.69sec$
$R_{G4}(pu)$	$0.00222\ \Omega$
$X_{G4}(pu)$	0.295 H
Base MVA	1000
Proposed control gains	$l = 1.35, k_{1a} = 1.13, k_{2a} = 1.31, k_{3a} = 1.223, k_{1b} = 3.23, k_{2b} = 0.84, k_{3b} = 2.13, \gamma_1 = \gamma_2 = \gamma_3 = 1.15$

Table 4.1. Specifications and Values of System Parameters

To examine the controller performance the following five cases are carried out.

- *Case 1:* Two cascading (same location) severe faults (three-phase) of duration 200 $msec$ at bus 33, connected to SG $G4$. The first temporary fault is applied at $t = 30\ sec$, followed by another at $t = 34\ sec$.
- *Case 2:* Two cascading (different location) severe faults at bus 14 and bus 33 of duration 0.2 sec are applied at $t = 30\ sec$ and $t = 60\ sec$, respectively.
- *Case 3:* Step perturbation in the mechanical input power at SG $G4$ is applied for 20 sec duration at $t = 30\ sec$.
- *Case 4:* The control coefficient T'_{do} of SG $G4$ is perturbed from 5.69 to 6 for 20 sec started at $t = 30\ sec$.

- *Case 5:* A wind farm renewable power source of 210 MW capacity is integrated from $t = 0\ sec$ on bus 33, and it is removed at $t = 25\ sec$.
- *Case 6:* One of the three phase transmission lines between bus 19 and bus 33 is temporally tripped at $t = 40sec$ for the duration $200msec$.

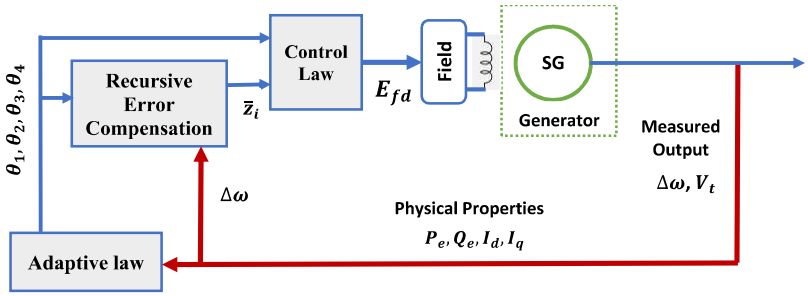

Figure 4.5. Block diagram showing the implementation of control of excitation system in the generator.

Case 1: In this case study, two cascading faults at the same bus are applied to analyze the control efficacy. The first fault occurs on bus 33 at $t = 30\ sec$, resulting in a corresponding line trip and subsequently low-frequency oscillation in the system. Before the oscillation due to the first events gets settled, the second three-phase short circuit fault is applied to study the controller performance under intense disturbance severity. The control input response using conventional PSSs design (PSS+AVR), ABC [42], and the proposed controller are shown in Figure *4.6*. This effectiveness of the proposed controller is achieved in terms of reduced control effort. The proposed scheme illustrates the response of adaptively tuned parameters as per (*4.36*) and (*4.45*) depicted in Figure *4.7*. The response of generator states is depicted in Figure *4.8*. Efficacy of the proposed scheme under cascading severe fault can be observed from these results. The response of the proposed control scheme is associated with quick settling time and reduced overshoot compared to the existing ABC scheme [42] and conventional PSSs.

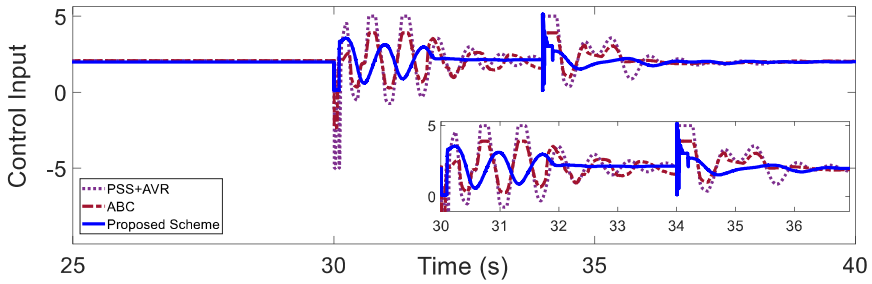

Figure 4.6. Control input response in case 1.

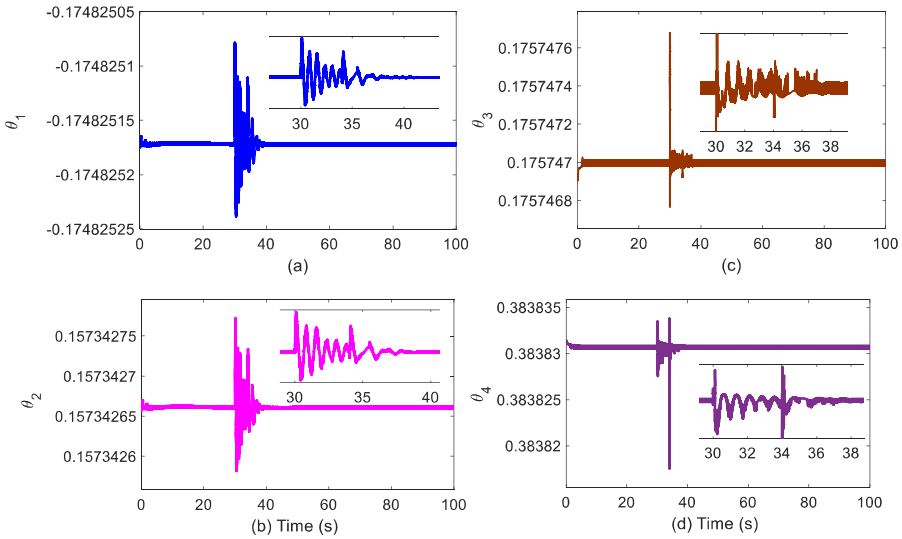

Figure 4.7. Adaptively tuned unknown parameters for the proposed scheme (a) θ_1 (b) θ_2 (c) θ_3 (d) θ_4.

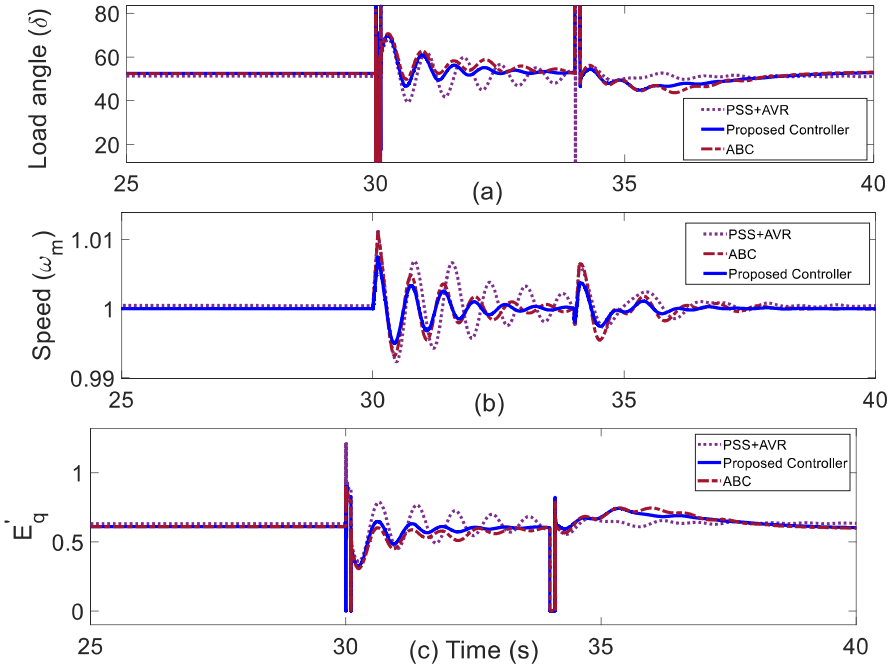

Figure 4.8. Generator $G4$ state responses in case 1 (a) δ (b) ω (c) E'_q

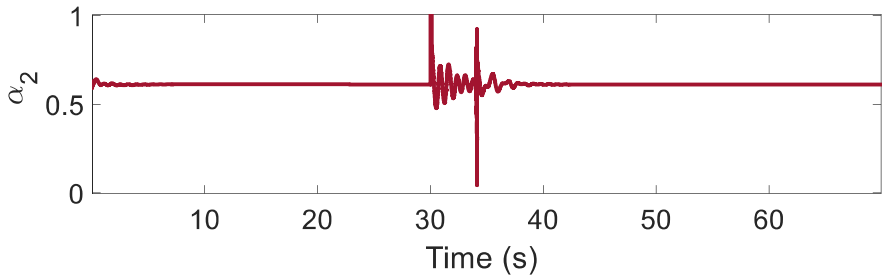

Figure 4.9. Virtual control input (α_2) response.

Virtual control response $\propto_2$ as expressed in (4.31) is obtained as depicted in Figure 4.9 for the case 1, which almost replicates the multimachine state E'_q. Response of the Nussbaum function (4.19) for the case 1 is provided in the Figure 4.10. Variation in the Nussbaum function is reflected as per perturbation case 1. The impact of sudden fault during the transient state of the system under the first fault is stabilized asymptotically by the controller using these functions, as illustrated in Figure 4.10.

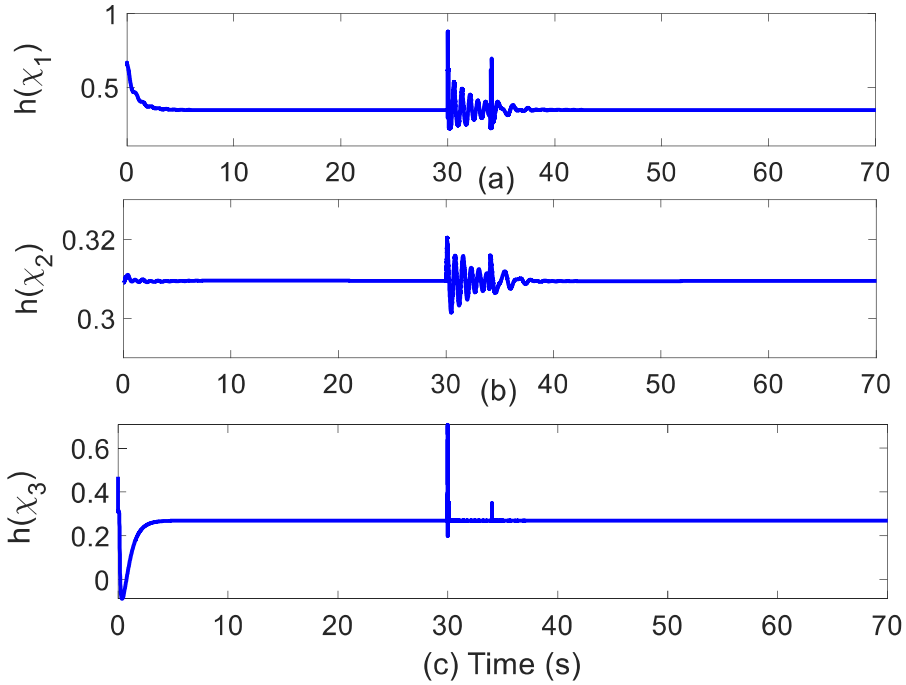

Figure 4.10. Response of Nussbaum functions (a) $h(\chi_1)$ (b) $h(\chi_2)$ (c) $h(\chi_3)$.

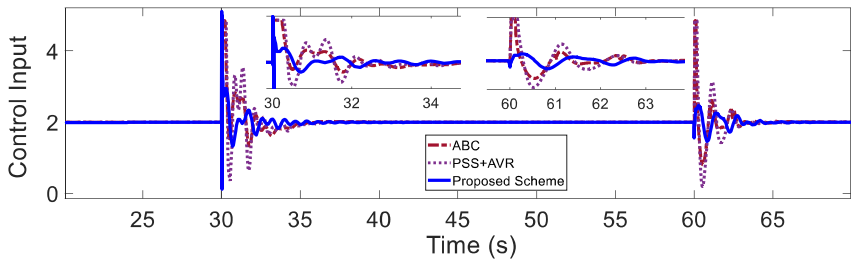

Figure 4.11. Control input response in case 2.

Case 2: Another severe cascaded short circuit fault is applied away from G_4 at bus 14 and near the generator G_4 at bus 33 respectively at $t = 30\ sec$ and $t = 60\ sec$. In this case, the severity of faults under the control schemes is analyzed. It is seen from the results shown in Figure 4.11 that the proposed control scheme required less control effort compared

with the ABC scheme [42] and PSSs due to simplified control expression and adaptation Nussbaum function present in the control law.

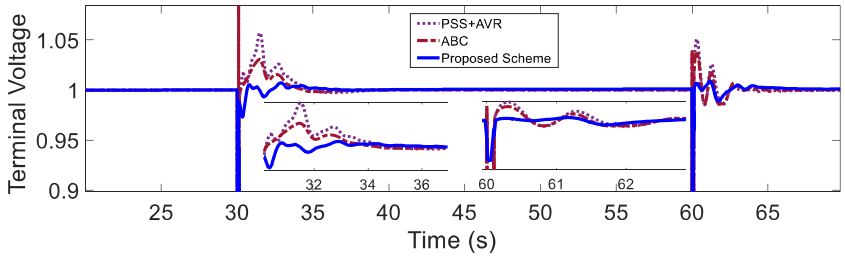

Figure 4.12. Terminal voltage response at the generator G_4.

Response of the terminal voltage of G_4 is illustrated in Figure 4.12. Adaptive tuning law developed in (4.36) and (4.45) for unknown parameters effectively adopt the impact of perturbation that occurred in the system, as illustrated in Figure 4.13. The smooth response with reduced oscillation is observed using the proposed scheme compared to the other two control techniques. The terminal voltage response reflects the impact of robust super twisting scheme having disturbance rejection capability. The generator state response is illustrated in Figure 4.14. It is seen that using the proposed scheme, the states are comparatively associated with reduced cycles of oscillation, along with low amplitude overshoot. It is observed that all states get stabilized and regain the equilibrium point faster than other control schemes. The state error response for this case is shown in Figure 4.15 as per (4.7), (4.8), and (4.9).

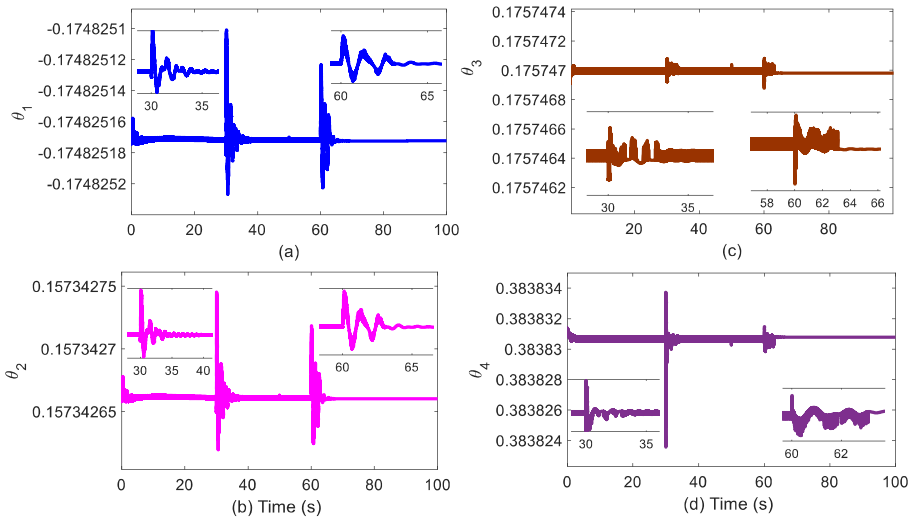

Figure 4.13. Unknown parameters of proposed scheme (a) θ_1 (b) θ_2 (c) θ_3 (d) θ_4.

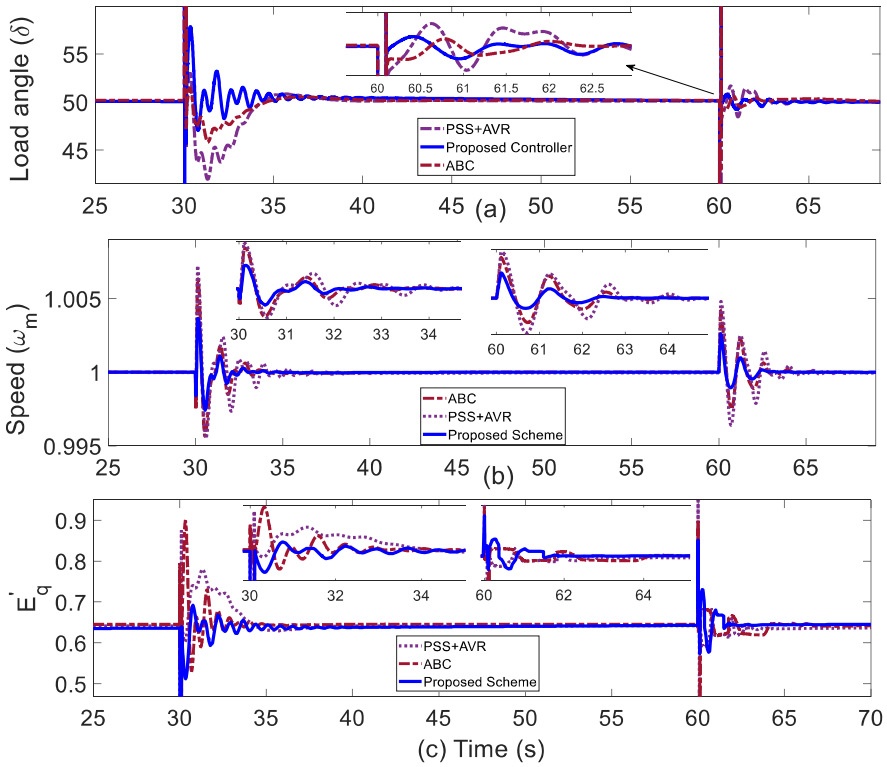

Figure 4.14. Generator $G4$ state responses in case 2 (a) δ (b) ω (c) E'_q.

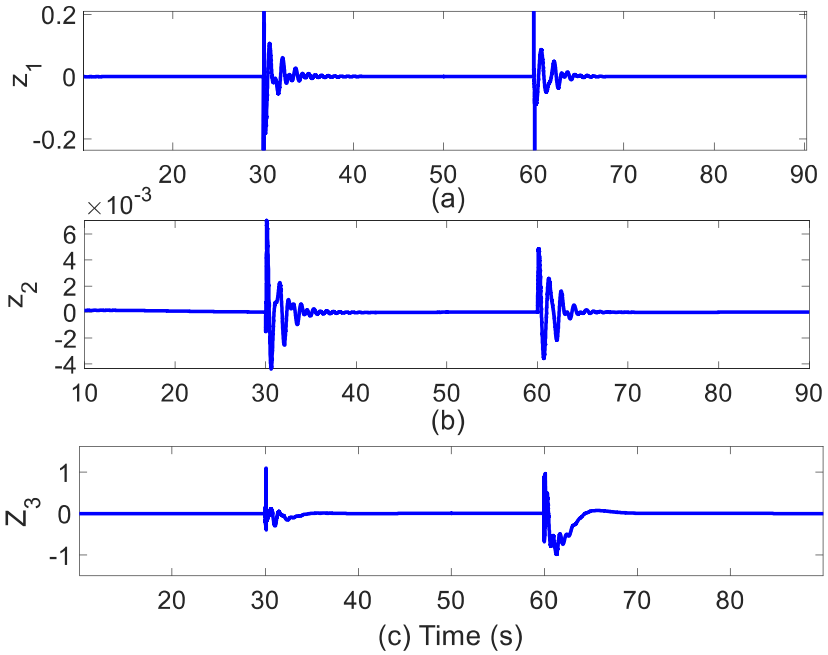

Figure 4.15. Response of state errors (a) z_1 (b) z_2 (c) z_3.

Case 3: Another intense disturbance is included by applying the 5% step change in the mechanical input power for a duration of 20 *sec* as depicted in Figure 4.16. The control action response, in this case, is represented in Figure 4.17. The reduced control effort is

observed in the result shown in Figure 4.17 as compared to the other two schemes. Virtual control action of $\propto_2$ as per (4.25) for this case is depicted in Figure 4.18. The generator G_4 states variation is shown in Figure 4.19. In this case the deviation of states from their initial state is observed during perturbed period. But the proposed control response reflects the minimum deviation, and reduced oscillations as compared to the ABC scheme [42] and PSSs during transient perturbation. It is observed due to reduced complexity in the control input and simplified adaptive laws for unknown parameters.

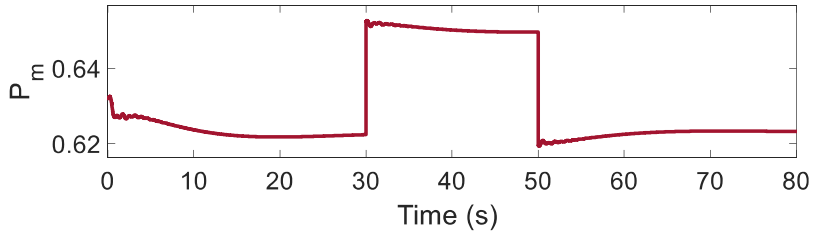

Figure 4.16. Perturbation in the mechanical input power (P_m).

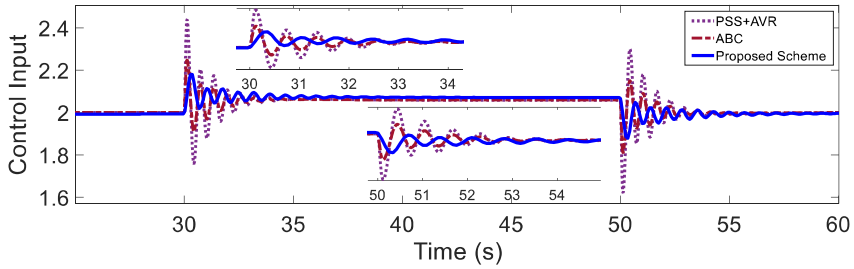

Figure 4.17. Control input response in case 3.

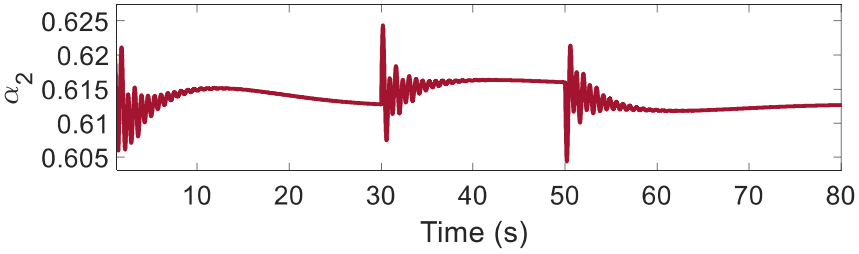

Figure 4.18. Virtual control input (α_2) response.

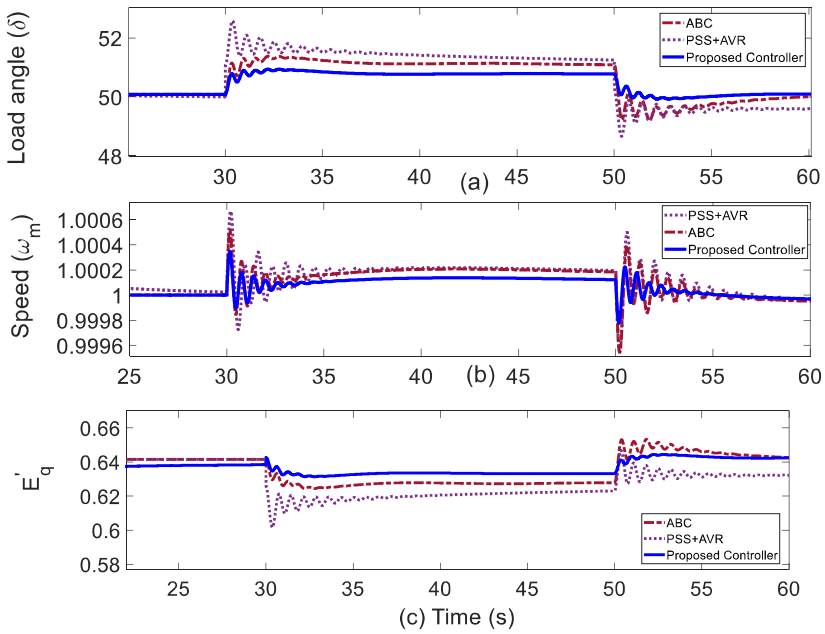

Figure 4.19. Generator $G4$ state responses in case 3 (a) δ (b) ω (c) E'_q.

Case 4: The impact of control coefficient variation is analyzed in this case study. Here the control coefficient T_{do} is varied from 5.69 to 6 for the period from $t = 30\ sec$ to $50\ sec$. Control input variation for all schemes is represented in Figure 4.20. The obtained result signifies that the Nussbaum functions suppress the variation in the control input as compared with the other two techniques. Spikes observed during perturbation indicate the boundedness of the control deviation. The response of unknown parameters for this case is illustrated in Figure 4.21. These adaptive parameters with control coefficient are varied according to adaptive law (4.36) and (4.45).

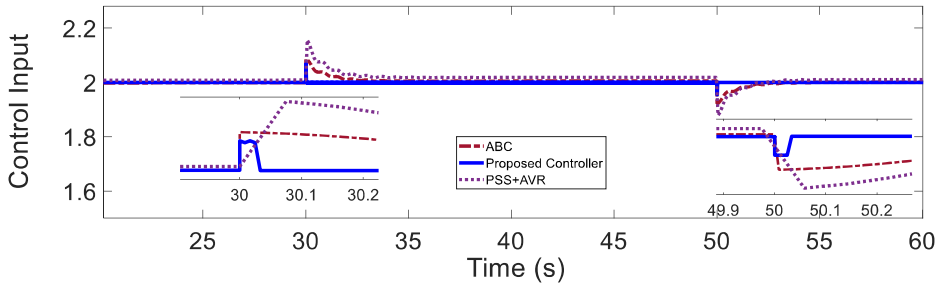

Figure 4.20. Control input response in case 4.

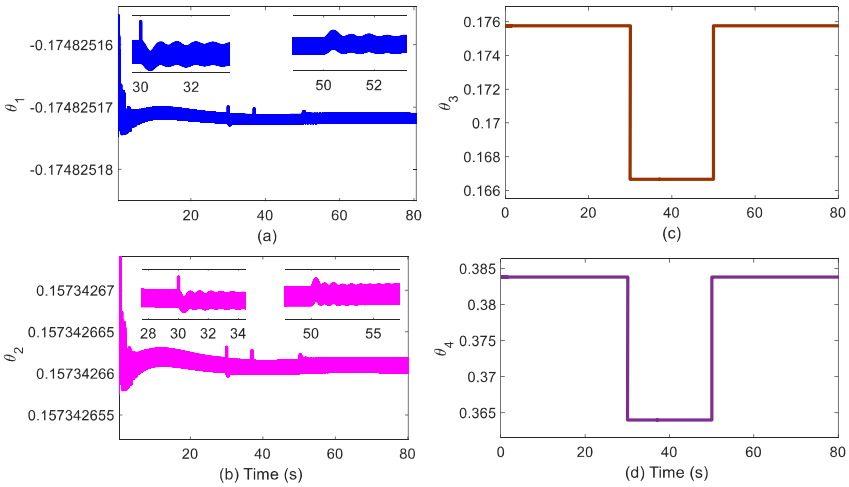

Figure 4.21. Unknown parameters of the proposed scheme (a) θ_1 (b) θ_2 (c) θ_3 (d) θ_4.

Case 5: In this case, the disconnection of renewable sources from the power network is analyzed. The wind farm of capacity 210 MW connected at bus 33 (near $G4$) is removed at $t = 25\ sec$ to perturb the system. The variation in the control signal under this case is shown in Figure 4.22. The variation in the voltage and current at the point of common coupling (PCC) is shown in Figure 4.23(a) and (b), respectively. The voltage drops at $t = 25\ sec$ in presence of load during wind farm removal, whereas the current at the PCC terminal is reduced to zero. The variation in wind turbine power can be observed in Figure 4.23(c). The Figure 4.23(d) shows the wind turbine rotor speed response and the active power of $G4$ is depicted in Figure 4.24.

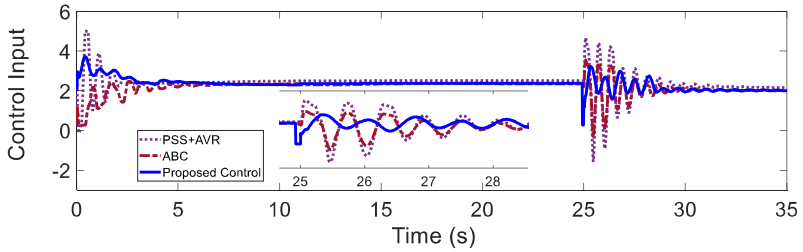

Figure 4.22. Control input response in case 5.

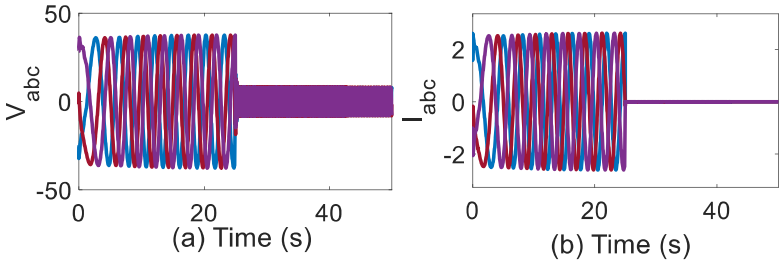

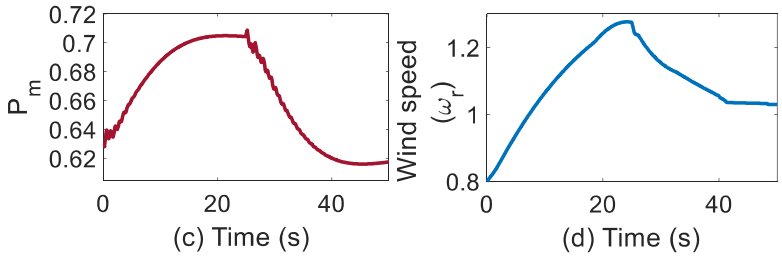

Figure 4.23. Responses in case 5, (a) PCC voltage (b) PCC current (c) Variation in P_m (d) Variation in the wind turbine rotor speed.

It can be observed that after removal of wind farm, active power response with the proposed scheme has fewer fluctuations. It signifies a better controller performance and exact estimation of parameters shown in Figure 4.25as compared to other schemes. The proposed adaptive law for unknown parameters causes small variations and reduced overshoot. On the other hand, the ABC scheme [42] has a large overshoot at the time of removal of wind farm as indicated in Figure 4.26. This efficacy in the proposed control response is obtained due to simplified adaptive tuning law and integration of super twisting scheme in the proposed control design.

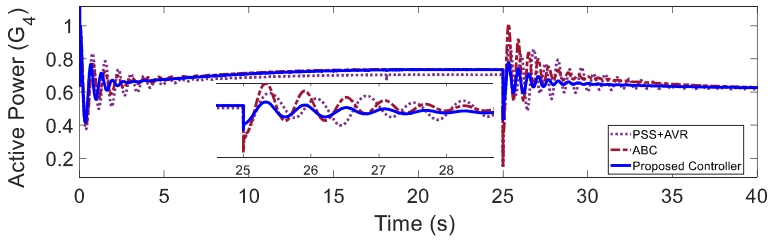

Figure 4.24. Electric power response at G_4.

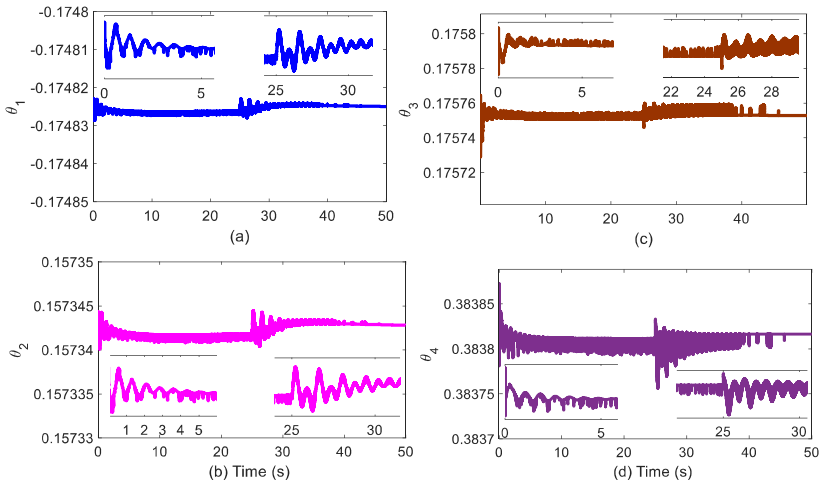

Figure 4.25. Unknown parameters of proposed scheme (a) θ_1 (b) θ_2 (c) θ_3 (d) θ_4.

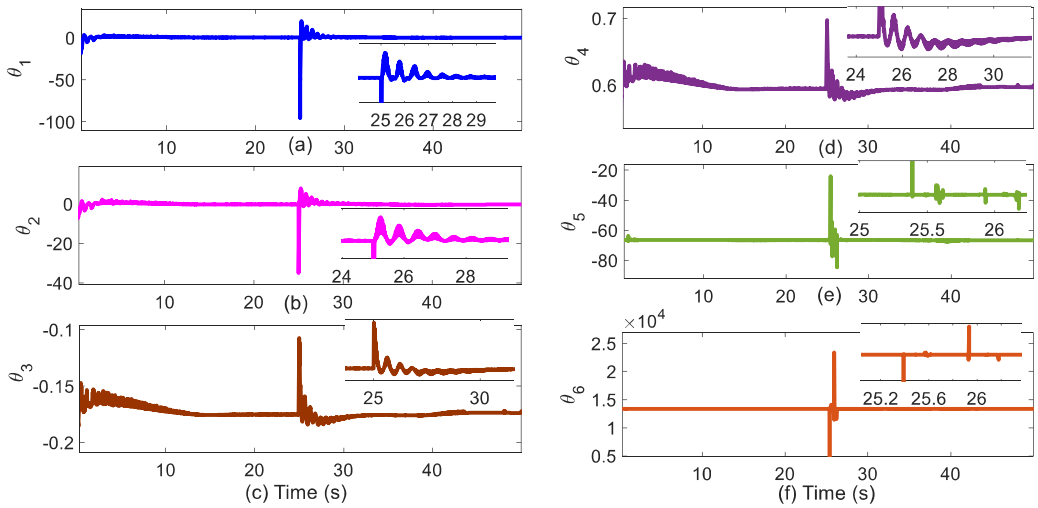

Figure 4.26. Unknown parameters for scheme [72] (a) θ_1 (b) θ_2 (c) θ_3 (d) θ_4(e) θ_5 (f) θ_6.

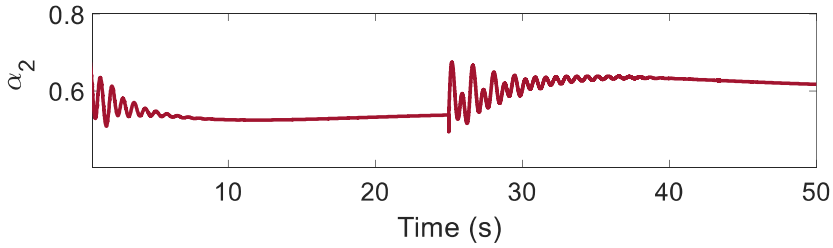

Figure 4.27. Virtual control input (α_2) response.

In this case, the control effort for the proposed control scheme is observed less as compared to ABC [42] and PSSs scheme. Response of virtual control signal $\propto_2$ according to (4.25), is illustrated in Figure 4.27. The stabilization of generator states is reflecting the proposed scheme's efficacy and are shown in Figure 4.28. The response using proposed scheme gets stabilized quickly and results in a reduced overshoot during convergence to their equilibrium point.

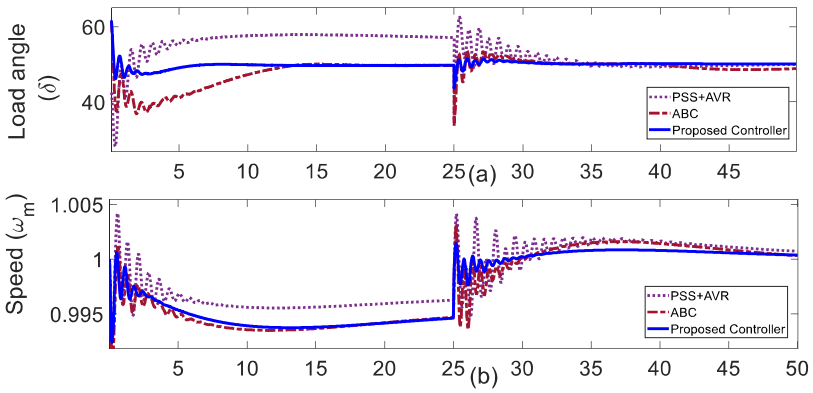

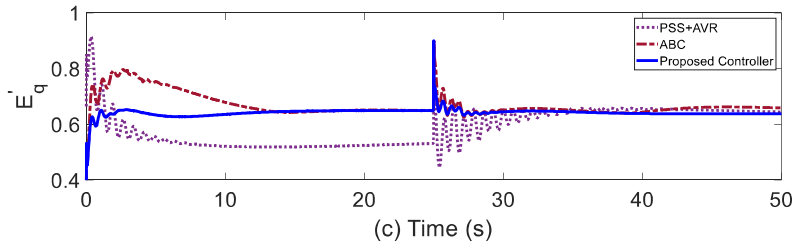

Figure 4.28. Generator $G4$ state responses in case 5 (a) δ (b) ω (c) E'_q.

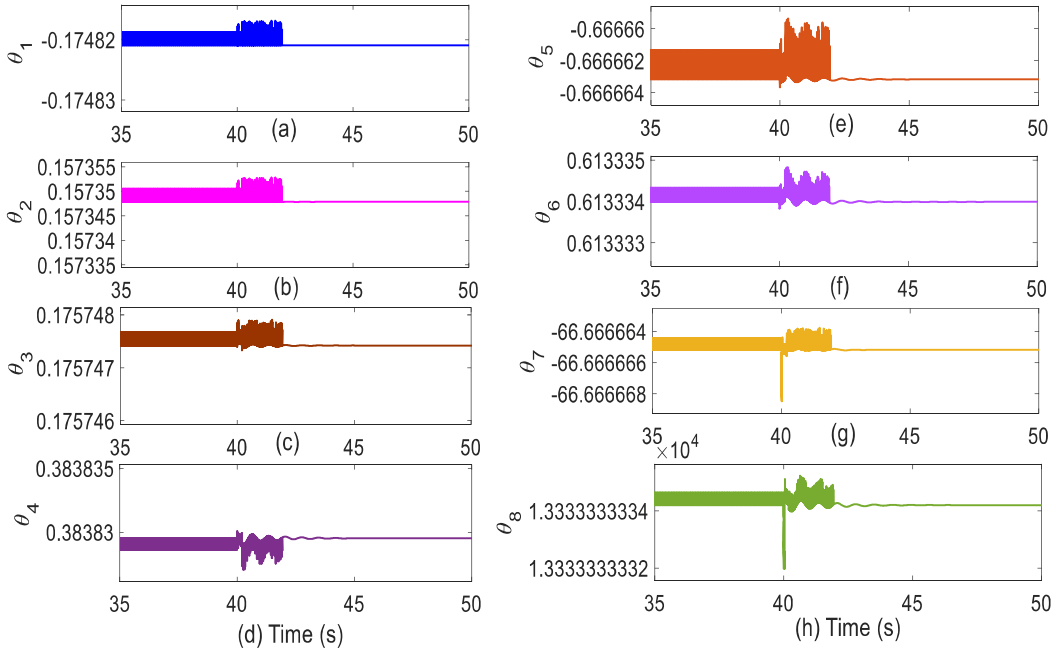

Figure 4.29. Response of adaptive parameters for higher order model (a) θ_1 (b) θ_2 (c) θ_3 (d) θ_4 (e) θ_5 (f) θ_6 (g) θ_7 and (h) θ_8.

Case 6: In this case, a comparative analysis is presented between adaptive PSSs scheme [85] and proposed scheme for higher order model. In this study one of the three phase transmission lines between bus 19 and bus 33 is temporally tripped at $t = 40sec$ for the duration 200 $msec$. The exciter parameters for both the schemes are provided in Table 4.2. The response of adaptive parameters obtained from proposed scheme are shown in Figure 4.29.

The Adaptive PSSs scheme is simulated as per the steps provided in Table 4.1 in [85]. The online updating of neuron weight law is taken from the equation (*4.27*) in [85] for the two neural network algorithms for step 8 and 11 respectively as provided in Table 4.1 of [85]. The corresponding estimated neural functions are provided in Figure *4.30*(a) and (b) respectively. All other system parameters are tuned accordingly. All the system state

responses are shown in Figure *4.31*. The obtained results show the fast stabilization of all states under proposed control scheme as compared with the adaptive PSSs scheme presented in [85]. The proposed scheme shows improved response due to the exact estimation of all adaptive parameters in the higher order model during perturbation. Transient overshoot response is improved in the proposed scheme under the influence of defined normalized function and barrier function with super twisting scheme.

Exciter Parameters

Specification	Value
Voltage regulator gain	$K_a = 200$
Voltage regulator time constant	$T_a = 0.015\ sec$
Maximum control element output	$V_{max} = 5\ volt\ (pu)$
Minimum control element output	$V_{min} = -5\ volt\ (pu)$
Exciter field resistance line slope margin, low pass filter (T_r)	$k_e = 1\ (pu), T_r = 0.02\ sec$
Transient gain reduction	$T_b = 10\ sec, T_c = 1\ sec$
Initial terminal and field voltage	$V_{t0} = 1volt\ (pu), E_{f0} = 2volt(pu)$

Table 4.2. Exciter Parameters

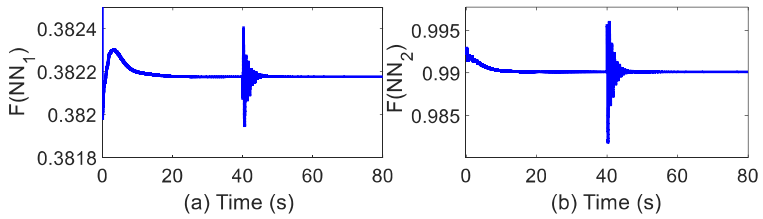

Figure 4.30. Estimated functions in adaptive PSSs scheme [85] (a) F (NN_1) (b) F (NN_2).

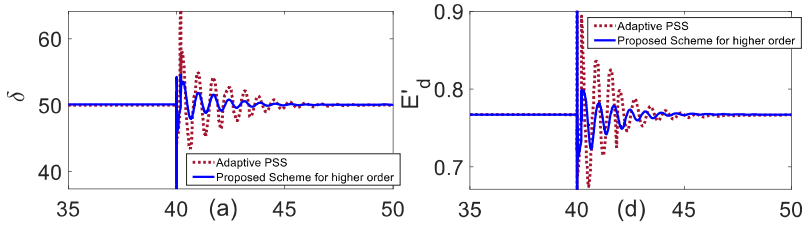

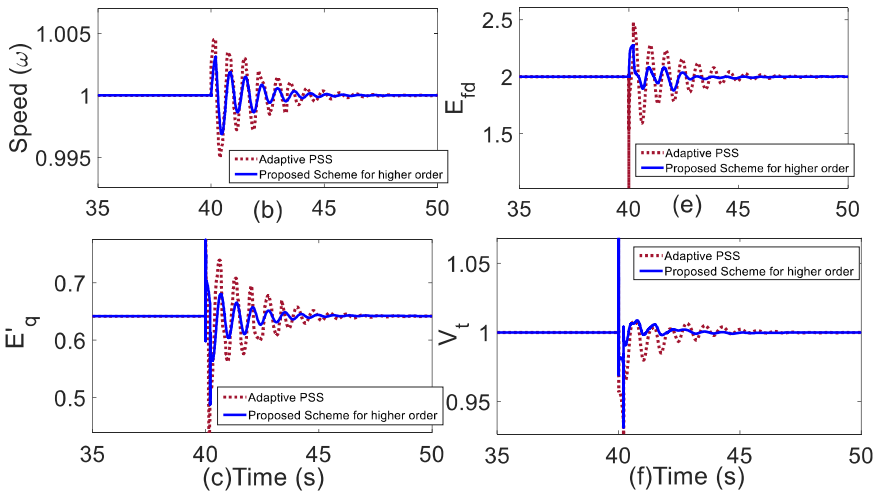

Figure 4.31. State responses of proposed scheme for higher order model and adaptive PSS scheme [85] (a) δ (b) ω (c) E'_q (d) E'_d (e) E_{fd} and (f) V_t.

4.5 Real-Time Validation of proposed scheme using RTDS Platform

The proposed approach is validated in real-time using RTDS as shown in Figure 3.30 in the Chapter 2. The RTDS is available in the smart grid lab at IIT BHU, Varanasi. The NovaCor RTDS is equipped with IBM POWER8TM CPU with four cores. It can do software in loop (SIL) operations with a frequency of 3.5 GHz. Each core in the RTDS NovaCor chassis can solve ninety nodes simultaneously using a PB5 style rack. The Simulink control block is converted into C codes. These codes are dumped in the C builder tool of RTDS. The control blocks built up by C codes in the C builder tool are linked to the IEEE 39 bus model in the RTDS. The RUNTIME tool in RTDS is used to execute the SIL. The block diagram representation of the SIL test is provided in Figure *3.31* in the Chapter 2. The following two real-time cases are performed in RTDS and compared with ABC [42].

1) Appling step load change at bus 20.
2) A three-phase short circuit fault applied on G_4 terminal, initiated at $t = 5\ sec$ for a duration of $0.2\ sec$.

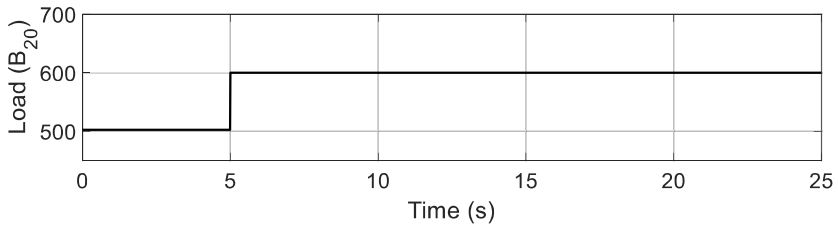

Figure 4.32. Step load change at bus 20.

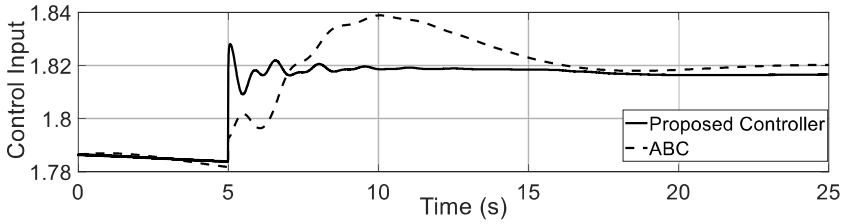

Figure 4.33. Control input response.

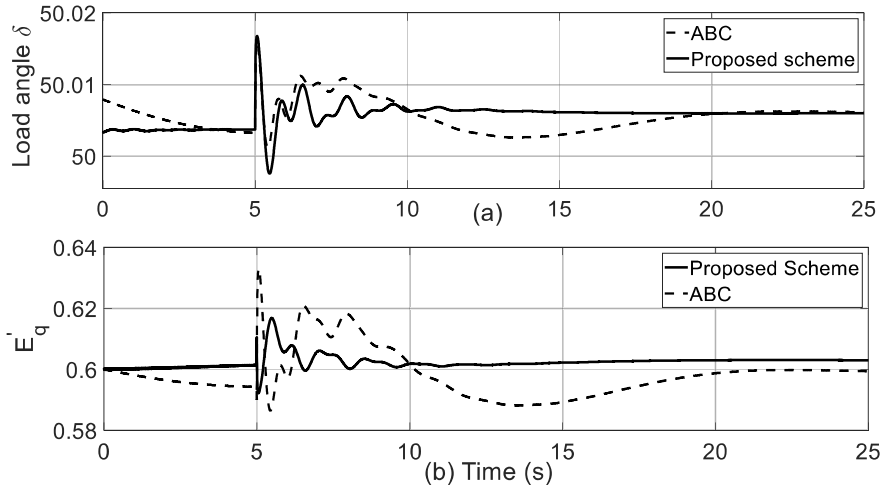

Figure 4.34. Generator $G4$ state responses (a) δ (b) E'_q.

In the first case, the operating condition of the power system model is varied by applying the step perturbation in the load at bus 20. The step-change in the load is shown in Figure 4.32. Control effort for this case is slightly shifted to other values to maintain the required effort for stabilization, as illustrated in Figure 4.33. It can be observed that the proposed control has a smooth response with reduced overshoot and fast convergence as compared to the ABC scheme [42]. A similar response is reflected in the variation of machine states as shown in Figure 4.34. These responses verify the significance of the super twisting and Nussbaum function in the proposed scheme as compared to ABC algorithm [42].

The second case of perturbation in real-time SIL test is applied at $t = 5\ sec$ with the three-phase short circuit fault of $0.2\ sec$. This severe fault is applied at G_4 terminal. The impact

of this severe fault on the control action is illustrated in Figure 4.35. Again from the Figure 4.35, the reduced control effort is observed as compared to ABC scheme [24]. Though, both control inputs have comparable effort, but the proposed scheme reflects better performance as seen in the obtained results. The generator state response is represented in Figure 4.36. These generator state responses using proposed scheme reflects the fast convergence to the equilibrium point, and reduced oscillations as compared to the ABC scheme [42]. The response obtained using proposed method has comparatively less overshoot. The effectiveness of the proposed scheme significantly enhances the power system stability regime in the domain of low-frequency oscillations.

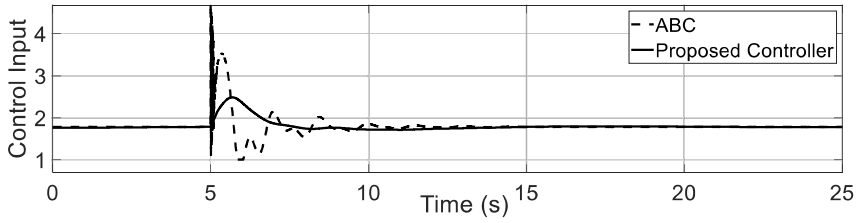

Figure 4.35. Control input response.

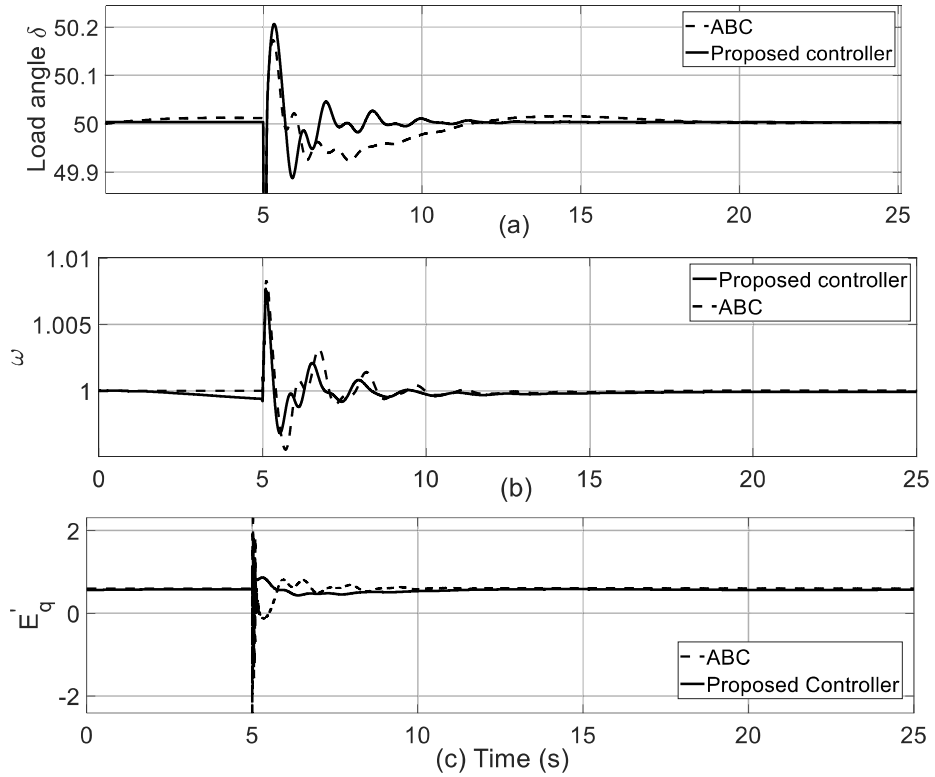

Figure 4.36. Generator $G4$ state responses (a) δ (b) ω (c) E'_q.

4.6 Summary

The proposed scheme with the Nussbaum function protected the control signal deviation within a specified bound during the changes in the unknown control coefficients. The super twisting law applied with the proposed scheme provided the strong robustness against external disturbances compared with recent schemes. The improved control performance was observed in results during perturbations, due to the elimination of residual error left in the recursive backstepping procedure. Also, the proposed scheme adequately addressed the adaptation law for unknown parameters with simplified expression, whereas in the other control schemes, complex expression of tuning laws presented with the number of internal states.